

# GC–MS Analysis of Amino Acids Rapidly Provides Rich Information for Isotopomer Balancing

Michael Dauner and Uwe Sauer\*

Institute of Biotechnology, ETH Zürich, CH 8093 Zürich, Switzerland

Gas chromatography–mass spectrometry (GC–MS) is a rapid method that provides rich information on isotopomer distributions for metabolic flux analysis. First, we established a fast and reliable experimental protocol for GC–MS analysis of amino acids from total biomass hydrolyzates, and common experimental pitfalls are discussed. Second, a suitable interface for the use of mass isotopomer data is presented. For this purpose, a general, matrix-based correction procedure that accounts for naturally occurring isotopes is introduced. Simulated and experimentally determined mass distributions of unlabeled amino acids showed a deviation of less than 3% for 89% of the analyzed fragments. Third, to investigate general properties of GC–MS-based isotopomer balancing, altered flux ratios through glycolysis and pentose phosphate pathway and/or exchange fluxes were simulated. Different fluxes were found to exert specific and significant influence on the mass isotopomer distributions, thus indicating that GC–MS data contain valuable information for metabolic flux analysis. Fourth, comparison of different methods revealed that GC–MS analysis provides the largest number of independent constraints on amino acid isotopomer abundance, followed by correlation spectroscopy and fractional enrichment analysis by nuclear magnetic resonance.

## Introduction

Precise monitoring of metabolic flux responses to genetic or environmental modifications provides meaningful insights into the phenotype of an organism and important information for rational metabolic engineering strategies (1). Initial metabolic flux analysis was solely based on metabolite balancing within the assumed or known bioreaction network stoichiometry. To obtain unambiguous solutions in the resulting, usually under-determined linear equation systems, artificial or experimentally unverified assumptions were necessary.

The availability of isotopic tracer data provides additional, independent information that can be used as constraints in flux calculations and thus offers an alternative to ad hoc assumptions. Most commonly,  $^{13}\text{C}$ -labeled substrates are used to produce labeled metabolites that are detectable by mass spectrometry (MS) or nuclear magnetic resonance (NMR) spectroscopy (2). Initial tracer experiments were based on the analysis of selected metabolites and intuitive interpretation of the obtained labeling pattern, condensed into analytically deduced equations. Recent advances enable a more comprehensive analysis of cellular metabolism by labeling pattern analysis in all proteinogenic amino acids (3, 4).

Similarly to metabolite balancing, balances can be set up around all isotope isomers (isotopomers) of a particular metabolite. By extending metabolite to isotopomer balances, a framework was introduced that allows mathematical description of flux relationships in complex central metabolic networks and labeling properties at the

same time (5–7). This formalism guarantees maximum information retrieval and permits the incorporation of NMR data from fractional enrichment (8) or correlation spectroscopy (9), as well as from mass distributions determined by gas chromatography (GC)–MS analysis (10).

Although experimentally simpler and cheaper, GC–MS has attracted much less attention than NMR. One reason may be that usually the isotopomer pool of a given metabolite is only partly determined by either method. However, GC–MS-derived constraints on isotopomer pools are difficult to interpret intuitively and require an abstract modeling framework. In contrast, NMR provides information on the position of the label in the carbon skeleton, which allows direct conclusions on the precursor composition (2). Compared to NMR, however, GC–MS analysis is much more sensitive (2) and involves simpler sample handling with little manual work, thus opening the door to miniaturization and high throughput analysis.

The isotopomer composition of metabolic intermediates is a function of the cell's flux state and depends on the reaction network, the administered label, and the metabolic state of the system (Figure 1). Isotopomer balancing seeks to identify the inverse function to access the flux state. If no analytical function is available, calculation of the inverse function may be approached by iterative fitting procedures. However, high turnover rates of metabolites and low concentrations present a problem for isotopomer analysis of central carbon pathways intermediates (2). To avoid this problem, the imprinted isotopomer composition of pathway intermediates is often analyzed in the amino acids (Figure 1), which are synthesized from these metabolites and are available at high concentrations in cellular protein. Thus, the bio-

\* Tel: +41-1-6333672. Fax: +41-1-6331051. Email: sauer@biotech.biol.ethz.ch.

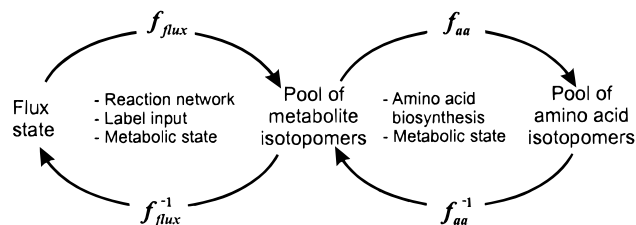


**Figure 1.** Relationship between the isotopomer distribution of amino acids, the isotopomer distribution of metabolites, and the flux state of a biological system.

synthetic pathways of amino acids and their metabolic state are underlying parameters if the inverse function is sought by metabolite balancing with amino acid data.

The aim of this work was to establish a simple and reliable GC-MS protocol for the determination of amino acid mass isotopomers, as well as a formalism to incorporate such data into an isotopomer modeling framework. The potential value of such mass isotopomer data for metabolite flux analysis by isotopomer balancing was investigated using model simulations. Moreover, unlabeled bovine serum albumin (BSA) or total *Escherichia coli* biomass were used to examine basic properties of the analytical method detached from the peculiarities of a biological system.

### Material and Methods

**Sample Preparation.** BSA (Sigma) was dissolved in water at different concentrations. *E. coli* cells were disrupted by sonication for 5 min, and cell debris was removed by centrifugation at 14 000 rpm for 5 min. Aliquots of 0.5 mL and a protein concentration between 0.1 mg/L and 100 mg/L were mixed with 1.5 mL of 6 M HCl in a 2.2 mL Eppendorf tube and incubated at 110 °C for 24 h. The hydrolyzates were dried under vacuum in a speedvac at room temperature for 12 h. For derivatization, the dried hydrolyzates were resuspended in 100  $\mu$ L of tetrahydrofuran (Fluka), 100  $\mu$ L of *N*-(*tert*-butyldimethylsilyl)-*N*-methyl-trifluoroacetamide (MTBSTFA) (Fluka) was added, and the mixture was incubated for 60 min at 60 °C. Protic sites of amino acids (OH-, NH-, and SH-groups) were blocked by silylation to reduce dipole-dipole interactions and to increase volatility for GC separation (11). The use of MTBSTFA had the advantage that mostly neutral and volatile byproducts are formed that did not react with the column, hence enabling direct GC-MS analysis (12).

**Gas Chromatography-Mass Spectrometry.** GC-MS was carried out using a HRGC Mega2 gas chromatograph (Fisons) equipped with a SPB-1 column (Supelco, 30 m  $\times$  0.32 mm  $\times$  0.255  $\mu$ m) that was directly connected to a MD800 quadrupole mass spectrometer (Fisons). The injection volume was 1  $\mu$ L at a carrier gas flow of 2 mL/min helium with a split ratio of 1:20. The initial oven temperature of 150 °C was maintained for 2 min and then raised to 280 °C at 3 °C/min. Other settings were 250 °C interface temperature, 200 °C ion source temperature, and electron impact ionization (EI) at 70 eV. Mass spectra were analyzed in the range of 60–650 atom mass units (amu) at a rate of 90 scans/min for a run time of 40 min. MS data were processed using the program MassLab from Fisons.

### Results

**Experimental Analysis.** Using a single-step derivatization of hydrolyzed BSA or total cellular biomass and GC analysis, we were able to detect 16 of the 20

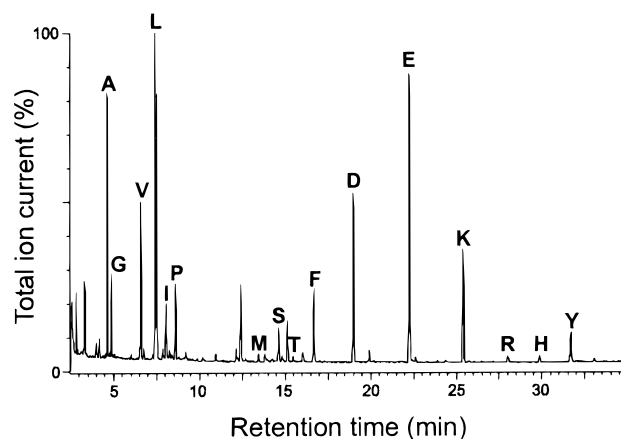


**Figure 2.** Gas chromatogram of hydrolyzed, TBDMS-derivatized BSA (250 mg/L). Detected amino acids are denoted with their one-letter symbol.

proteinogenic amino acids (Figure 2). Cysteine and tryptophane were oxidatively destroyed during acid hydrolysis, and asparagine and glutamine were deamidated to aspartate and glutamate, respectively, (13).

During GC separation, an undesired isotope fractionation of the derivatized amino acids was observed. Depending on the total mass, molecules of higher masses were eluted first from the capillary column. This manifests itself in a constant decrease of heavier and increase of lighter mass isotopomer over the scans for a particular amino acid (Figure 3), as was described previously (14, 15). To obtain meaningful mass isotopomer ratios that are not biased by this fractionation, every mass isotopomer signal was integrated over the full peak range of the corresponding amino acid. Compared to the determination of mass isotopomer ratios only at the peak of a molecule's signal, this integration of all signals results in a much lower signal-to-noise ratio that disables the use of low abundance fragments.

Theoretically expected mass fragments were examined, and overlapping fragments were excluded from further analysis. Typical cracking patterns of TBDMS-derivatized amino acids are shown schematically in Figure 4. None of the 16 detected amino acid exhibited a significant molecular ion signal  $M^+$  that represents the completely derivatized amino acid. Loss of a methyl or a *tert*-butyl group of the *tert*-butyldimethylsilyl (TBDMS) substituent yielded the fragments  $(M - 15)^+$  or  $(M - 57)^+$ , which still contain the complete amino acid. Another frequently observed signal originated from the  $(M - 85)^+$  fragment. This ion is assumed to result from the fragments  $(M - 15)^+$  and  $(M - 57)^+$  by rearrangement under loss of CO (16). Other occurring fragments were  $(M - 159)^+$ , originating from the loss of C(O)-O-TBDMS,  $f302^+$ , resulting from a broken bond between the  $\alpha$ - and  $\beta$ -carbon atom of the amino acid, and the corresponding side chain  $(sc)^+$  with varying masses for each amino acid.

Quantitative accuracy of the measurements is of utmost importance for mass isotopomer analysis (17). One potential cause of inaccuracy is incomplete resolution of adjacent ions in the ion envelope, due to ion scattering and peak tailing (18). Therefore the mass spectrometer (lens system, quadrupole prefilters and main rods, detector) was tuned thoroughly at the beginning and during the analysis using mass isotopomer standards to maintain optimum mass-resolving capacity. A second source for inaccuracy may be nonlinearity of the detector response at different mass isotopomer ratios or different sample concentrations (17). While Bergner and Lee (19)

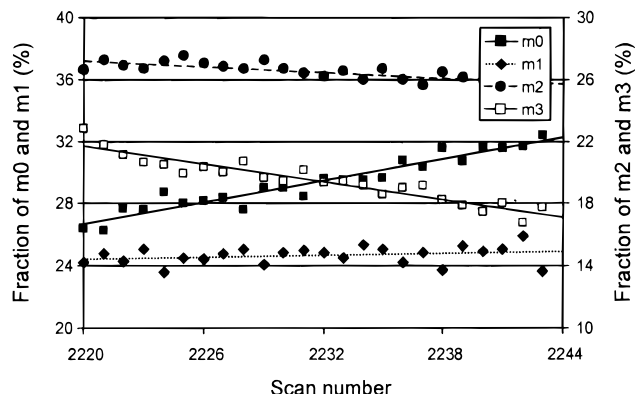


**Figure 3.** Isotope fractionation during GC separation for the example of the  $(M - 57)^+$  fragment of glutamate.  $m_0$  denotes the base mass fragment containing no isotopes,  $m_1$  to  $m_3$  indicate mass isotopomer fractions that are 1 to 3 atom mass units heavier, respectively.

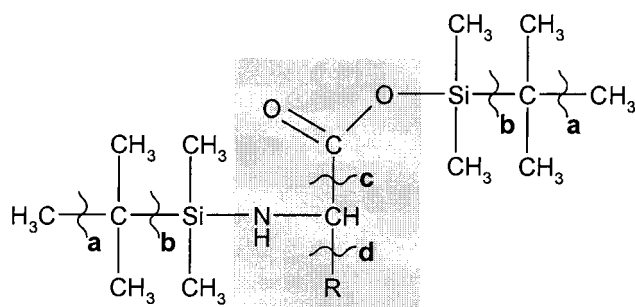


**Figure 4.** The most prominent detected fragments of TBDMS-derivatized amino acids. The amino acid with the specific side chain (R) is in gray. Cracking at the denoted positions yields the following fragments: a,  $(M - 15)^+$  and methyl group; b,  $(M - 57)^+$  and *tert*-butyl group; c,  $(M - 159)^+$  and  $C(O)O$ -TBDMS ion; d,  $(f302)^+$  (the double silylated  $C_1$ - $C_2$  fragment) and the side chain  $(sc)^+$ , consisting of R and possibly further TBDMS groups.

reported mass isotopomer ratios of different deuterated glucose that were invariant over a wide concentration range, Fagerquist et al. (20) observed a disproportional correlation between mass isotopomer ratios and sample size of fatty acid methyl esters. Thus, we examined mass isotopomer ratios of naturally labeled TBDMS-amino acids in a concentration range of 3 orders of magnitude. However, the mass isotopomer ratio was not effected by the sample size, provided no significant overlap of the mass isotopomer peaks occurred and the signal did not exceed the upper detector limit.

Amino acid concentrations in hydrolyzates are difficult to predict because they are a function of various factors, including protein concentration, degree of hydrolysis, stability, and probability of fragment occurrence. Thus, sample concentrations cannot always be adjusted to meet the optimum measurement conditions prior to analysis and may exceed the detector limit. In such cases, the measured signal remains at its maximum value and its isotopomer fraction will, therefore, be underestimated and yield false results. This effect is identified by an inhomogeneous peak composition as exemplarily shown in Figure 5. In our particular case, such detector overload effects were seen at a measured ion current of about  $3 \times 10^9$  ions/(amu·s). In such cases, samples were diluted with THF to remain in the appropriate range and analyzed again. During the first analysis step, deviations caused by column bleeding were considered by subtracting the signals of a THF sample without amino acids from the fragment signals obtained. Additionally, every chro-

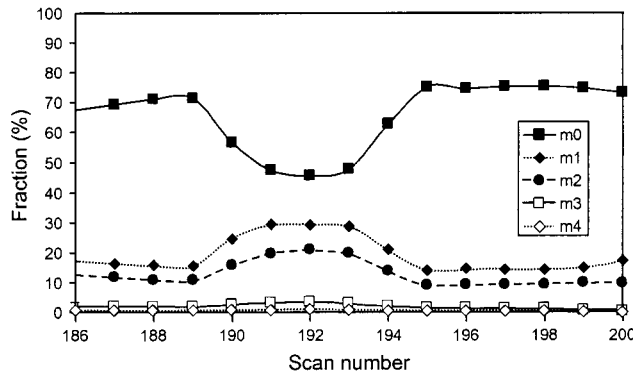


**Figure 5.** Influence of the detector limit on the signal determination of mass fragments by MS at the maximum intensity. The example shown here is the mass distribution of the  $(M - 159)^+$  fragment of alanine.

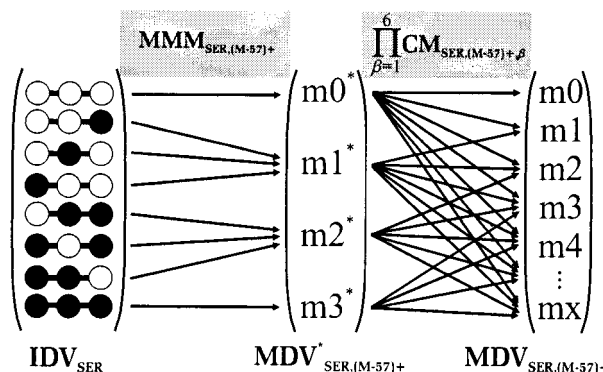


**Figure 6.** Correlation between isotopomer and mass isotopomer distribution, represented by the IDV and MDV, illustrated for the serine  $(M - 57)^+$  fragment. The eight possible isotopomers of the C3 carbon skeleton of serine constitute 4 mass isotopomers. The skewing effects of additional elemental isotopes must be considered by correction matrices. In our procedure, the conversion between the IDV and the MDV is achieved by a one-step matrix multiplication by  $MMM_{SER,(M-57)^+}$ .

matogram was examined for peak tailing, drifting base-lines, and suboptimal integration, and if necessary, integration was adjusted manually.

**Calculation of Isotopomer Distributions from Mass Data.** The use of isotopomer balances in metabolic flux analysis employs combinatorial probability analysis and requires detailed knowledge on the fates of carbon atoms. The production rate of a specific isotopomer depends on the probability of its formation, which, in turn, depends on the formation probabilities of its precursor metabolites and on the actual metabolic flux ratios, assuming the absence of isotopic effects (6). The resulting complex equation systems are conveniently handled using matrix calculus (7, 21), wherein an isotopomer distribution vector (IDV) represents the isotopomer composition of each metabolite. This principle can simply be extended to describe the isotopomer composition of each amino acid (*aa*). The transformation of an IDV into the corresponding mass distribution vector (MDV) of a fragment  $\alpha$  (Figure 6) can be achieved using mass mapping matrices ( $MMM$ ) (22) according to eq 1. A  $MMM$ , there-

$$MDV_{aa,\alpha}^* = MMM_{aa,\alpha}^* \cdot IDV_{aa} \quad (1)$$

fore, contains information on the corresponding mass of isotopomer fragments of each amino acid.

Additionally, naturally occurring elemental isotopes must be considered (Figure 6). This can be achieved by subsequent multiplication of the  $MMM^*$  by correction

matrices (CMs) for all relevant elements of number  $n$ , with each CM representing the statistical skewing effect of the  $\beta$ th element according to its isotope distribution:

$$\text{MMM}_{aa,\alpha} = \text{MMM}_{aa,\alpha}^* \cdot \prod_{\beta=1}^n \text{CM}_{aa,\alpha,\beta} \quad (2)$$

The CMs were constructed by simulating all elemental isotopologues that are defined by an position-independent isotopic composition. Thus, isotopologue have a unique mass but may not have a unique structure. With the number of all possible isotopes  $q_{\alpha,\beta}$ , the probability of their occurrence was determined according to

$$\text{prob}(\chi_{\alpha,\beta}^*) = \prod_{i=0}^{q_{\alpha,\beta}-1} p_{\beta}(i+1)^{\chi_{\alpha,\beta}^{(i+1)}} \cdot \frac{(m_{\alpha,\beta} - \sum_{j=1}^i \chi_{\alpha,\beta}(j))!}{(m_{\alpha,\beta} - \sum_{j=1}^{i+1} \chi_{\alpha,\beta}(j))! \cdot \chi_{\alpha,\beta}(i+1)!} \quad (3)$$

with  $p_{\beta}(i)$  being the natural abundance and  $\chi_{\alpha,\beta}(i)$  the number of atoms of the  $i$ th isotope of the  $\beta$ th element, whereas  $m_{\alpha,\beta}$  represents the total number of atoms of the  $\beta$ th element. The probabilities of equal masses of different isotope constitutions were then summed, resulting in the overall probability of a certain mass shift.

**Simulations.** To demonstrate the potential of GC-MS analysis for metabolic flux analysis and to examine characteristic features of mass isotopomer analysis, we constructed a simplified model consisting of glycolysis and pentose phosphate pathway (PPP) (Figure 7). Exchange fluxes were allowed only in the reactions catalyzed by transketolases (TK) and transaldolase (TA), whereas all other reactions were considered unidirectional. Linear reaction sequences were lumped into a single reaction step. Ribulose 5-phosphate, ribose 5-phosphate, and xylulose 5-phosphate, as well as dihydroxyacetone phosphate and glyceraldehyde 3-phosphate, were assumed to be in rapid equilibrium (23) and thus were treated as homogeneous metabolite pools, C5 and T3P, respectively. Additionally, precursor requirements for biomass formation were also considered (24). For simplicity, corrections for skewing effects of other natural isotopes were not included. Using a mixture of 10% uniformly, 40% C<sub>1</sub>, and 50% naturally labeled glucose as the substrate, the mass isotopomer distribution of the (M - 57)<sup>+</sup> and (f302)<sup>+</sup> fragments of serine were simulated at different assumed split ratios of fluxes through glycolysis and PPP (1:0; 1:1; 0:1). At each split ratio, individual or simultaneous activity of the TK and TA reactions at the rate of glucose uptake was simulated. For simplicity, serine was assumed to originate exclusively from PGA.

Independent of the exchange fluxes, almost all mass isotopomer fractions show significant variations depending on the glycolysis-to-PPP split ratio, most pronounced for the m1 fraction of the (M - 57)<sup>+</sup> fragment of serine (Figure 8). The lower proportion of this m1 fraction at higher PPP fluxes is explained by the loss of labeled C<sub>1</sub> in the decarboxylation reaction of the oxidative PPP, which, in this particular model, is the only reaction through which labeled carbon atoms can exit the system. With increasing PPP fluxes, the fraction of fully labeled T3P molecules decreases and fragments labeled at positions C<sub>1</sub> and C<sub>2+3</sub> are formed by mixing of fully and unlabeled C<sub>2</sub> and C<sub>3</sub> units in the non-oxidative PPP. This

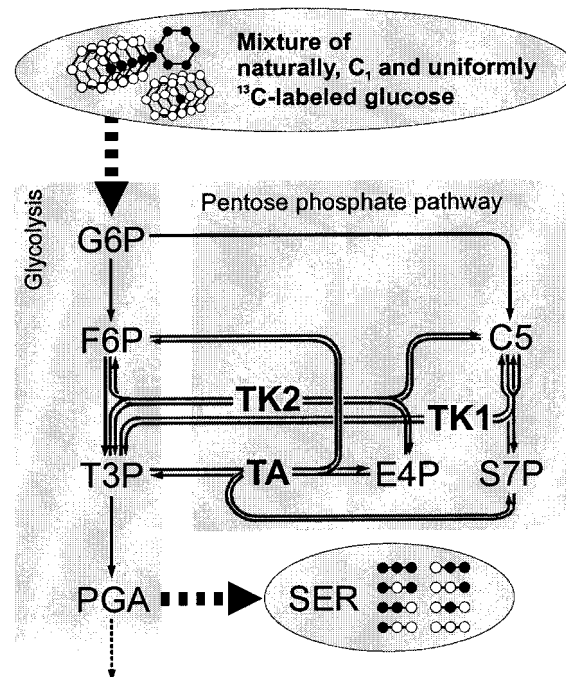


**Figure 7.** Simplified isotopomer model of glycolysis and pentose phosphate pathway. Abbreviations: G6P, glucose-6-phosphate; F6P, fructose-6-phosphate; T3P, triose-3-phosphate; C5, pentose-5-phosphate pool; S7P, seduheptulose-7-phosphate; E4P, erythrose-4-phosphate; PGA, 3-phosphoglyceric acid; SER, serine. Gray arrows indicate reversible reactions.

manifests itself in a decreased m3 and an increased m2 fraction, as well as a decreased m2 and an increased m1 fraction of the (M - 57)<sup>+</sup> and (f302)<sup>+</sup> fragments, respectively.

While exchange fluxes in TK1 or TA have almost no effects, the TK2 exchange fluxes generate increased m2 fractions of the (M - 57)<sup>+</sup> and m1 of the (f302)<sup>+</sup> fragments if the PPP is not operating at 100%. This can be explained by increased formation of C<sub>1</sub>-, C<sub>1+3</sub>-, and C<sub>2+3</sub>-labeled molecules at the expense of C<sub>3</sub>- and C<sub>1-3</sub>-labeled molecules. If all three exchange fluxes operate simultaneously, additional C<sub>2</sub>-labeled T3P molecules arise. Generally, compared to the (M - 57)<sup>+</sup> fragment, the m1 and m2 mass isotopomer fractions of the (f302)<sup>+</sup> fragment show the opposite trend in almost all cases. This is due to the loss of the hydroxymethyl group that corresponds to the C<sub>1</sub> carbon of glucose if metabolized via glycolysis.

These results allow for several conclusions: (i) The mass distribution of isotopomers can change significantly upon variations in the flux state of a metabolic system and thus contains information on both net and exchange fluxes. This information is not only contained in complete mass isotopomer spectra but also in partial ones (in the minimal case as the ratio of two mass isotopomers). (ii) The generation of different fragments in the cracking process is desirable because such fragments provide further information on the mass isotopomer distribution of a given metabolite and thus the flux state. Hence electron impact ionization is an advantageous procedure that generates complex mass spectra. Fragments yielding independent, redundant labeling information are useful for statistical data analysis. (iii) In most complex flux systems, isotopomer/mass isotopomer analysis does not allow the explicit resolution of all fluxes under all conditions, because the mass isotopomer distribution of a given set of fragments may be generated by different combinations of fluxes.

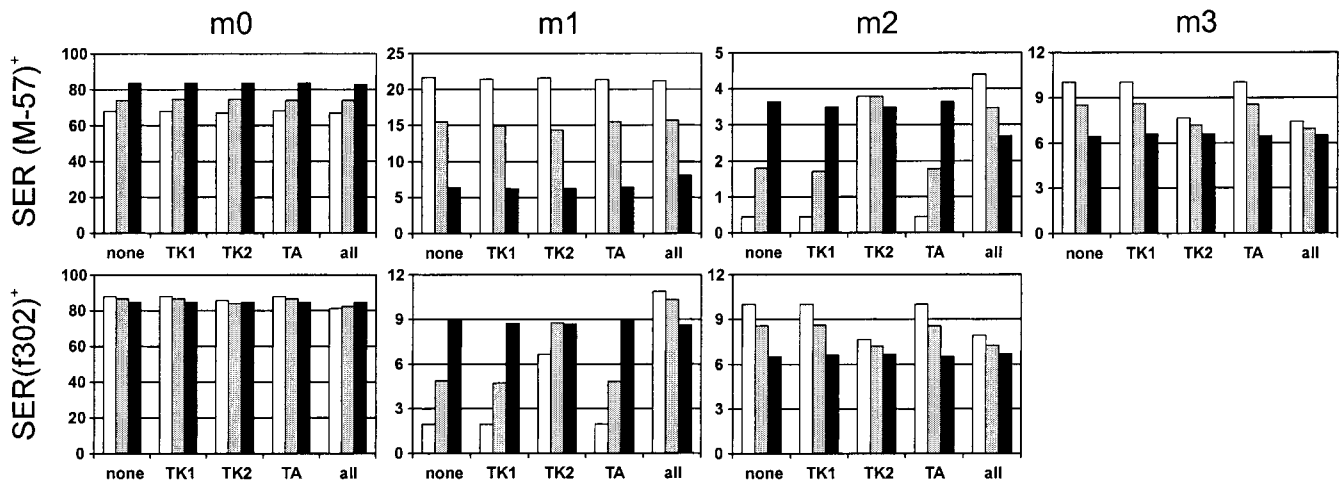


**Figure 8.** Mass isotopomer distribution of the  $(M - 57)^+$  and  $(f302)^+$  fragments of serine at glycolysis-to-PPP split ratios of 1:0, 1:1, and 0:1, indicated by the white, gray, and black bars, respectively. Exchange fluxes equaling the glucose uptake rate were considered to be absent (none), present in only one of the transketolase and transaldolase reactions (TK1, TK2, or TA), or present in all three reactions (all). Mass isotopomer fractions ( $m_x$ ) of the carbon skeleton are given in percent without correction for skewing effects of elemental isotope.

**Correlation of Simulated and Experimentally Determined Results.** The signals of the 16 experimentally detected amino acids in BSA labeled at natural abundance (Figure 2) were simulated. To compare experimentally detected and computed results, the mass isotopomers of each fragment were normalized to the  $m_0$  fraction. All experimentally determined signals with a higher than 7% sum difference of the  $m_1$  and  $m_2$  fractions compared to the  $m_0$  fraction were discarded. All fragments of histidine and threonine were omitted because their signal-to-noise ratio was too low, probably as a consequence of their low concentration, and arginine was omitted because rearrangements obscured its cracking patterns. Furthermore, analytical artifacts (17) due to fragment ions, such as the extraction of H from the parent ion, were identified by thorough inspection of spectra and discarded. Thus, 38 fragments in the unlabeled BSA example from a total of 75 detected fragments were used for further analysis and are principally available for metabolic flux analysis (Table 1). Very similar results were obtained with hydrolyzed total biomass of unlabeled *E. coli* (data not shown). Generally, a good agreement was found (Table 1) with more than 68% of the accepted fragments ( $m_0$  fragments not accounted for) deviating less than 1% from the calculated signals, 89% less than 3%, and more than 97% less than 5%.

While natural isotope abundances may slightly deviate from literature values, for example for  $^{13}\text{C}$  by less than 0.05% in mammalian systems (25), variations in this range are negligible for isotopomer balancing because the influence on mass isotopomer distribution is much less than the influence of different flux regimes. Moreover, the final flux estimates result from balancing of all available isotopomer data, and a deviating isotope abundance would not affect all mass isotopomer distributions in the same fashion. Thus, the fitting procedure would very likely account for this influence. An artificial enrichment of isotopes that exceeds the negligible natural deviations may be caused, for example, by the manufacturing process of the derivatizing agent. This, however, can easily be identified using naturally labeled samples as a standard.

**Accessible Constraints on Isotopomer Abundance.** Unless applied to the identical case, the resolution of fluxes by different labeling pattern analyses is

difficult to assess or compare. Moreover, when applied to a particular biological system, the conclusions are valid only for the particular case and may not be generalized. The number of independent constraints on the isotopomer distribution, on the other hand, provides a rough indication for the information content of different methods and is used here for comparison of GC-MS analysis with other, NMR-based isotopomer analyses (3, 8). To resolve the abundance of all  $2^n$  isotopomers of an amino acid with  $n$  carbons from a linear equation system,  $2^n$  independent constraints are required. To deduce the number of independent constraints from experimentally detected fragment mass spectra, two aspects have to be considered: (i) An amino acid fragment comprising  $n$  carbon atoms may be labeled with up to  $n$   $^{13}\text{C}$  nuclei, i.e., the molecular mass detected in MS may range from  $m_0$  (only  $^{12}\text{C}$  atoms) to  $m_0 + n$  (only  $^{13}\text{C}$  atoms). Depending on the isotope composition of the other contained elements and the additional carbon atoms of the derivatizing agent, even  $m_0 + m$  mass isotopomer distributions can be observed, with  $m \geq n$ . If all  $m$  mass isotopomers are detected, still only  $n + 1$  constraints on the carbon isotopomer pool of the amino acids can be extracted, whereas the other  $m - n$  measurements provide redundant information that may be used to estimate the natural abundance of other elemental isotopes. (ii) During mass isotopomer detection, amino acids often break into several fragments that yield additional information on labeled carbon positions. However, the independent constraints on these different fragments cannot simply be summed, because some of them are linearly dependent.

To extract the number of independent constraints on the isotopomer distribution of the amino acids that can be extracted from the experimental GC-MS fragments (Table 1), the single linear equation systems of all measured fragments  $\alpha_1 - \alpha_n$  of the amino acid  $aa$  (eq 1) were combined to yield a single equation system

$$\begin{bmatrix} \text{MDV}_{aa,\alpha_1} \\ \text{MDV}_{aa,\alpha_2} \\ \vdots \\ \text{MDV}_{aa,\alpha_n} \end{bmatrix} = \begin{bmatrix} \text{MMM}_{aa,\alpha_1} \\ \text{MMM}_{aa,\alpha_2} \\ \vdots \\ \text{MMM}_{aa,\alpha_n} \end{bmatrix} \cdot \text{IDV}_{aa} \quad (4)$$

**Table 1. Accepted Experimentally Determined (exp) and Simulated (sim) Fragment Mass Isotopomer Distributions of TBDMS-Substituted Amino Acids from a BSA Sample**

amino acid	fragment	origin	m0 <sup>a</sup>	m1	m2	m3	m4	m5	m6	amino acid	fragment	origin	m0 <sup>a</sup>	m1	m2	m3	m4	m5	m6	m7	m8	m9	
Ala	(M - 57) <sup>+</sup>	exp:	1.000	0.238	0.098	0.017					Met	(M - 57) <sup>+</sup>	exp:	1.000	0.300	0.154	0.000	0.044	0.024				
		sim:	1.000	0.233	0.096	0.015					Met	(M - 57) <sup>+</sup>	sim:	1.000	0.264	0.148	0.029	0.008	0.001				
	(M - 85) <sup>+</sup>	exp:	1.000	0.221	0.089							(M - 85) <sup>+</sup>	exp:	1.000	0.258	0.153	0.000	0.026					
		sim:	1.000	0.222	0.091							(M - 85) <sup>+</sup>	sim:	1.000	0.253	0.143	0.027	0.007					
Asx	(M - 159) <sup>+</sup>	exp:	1.000	0.146	0.075							(M - 159) <sup>+</sup>	exp:	1.000	0.185	0.095	0.000	0.000					
		sim:	1.000	0.148	0.045							(M - 159) <sup>+</sup>	sim:	1.000	0.178	0.094	0.013	0.003					
	(M - 57) <sup>+</sup>	exp:	1.000	0.352	0.171	0.041	0.015				Phe	(M - 85) <sup>+</sup>	exp:	1.000	0.297	0.109	0.024	0.010	0.005	0.003	0.003	0.009	0.000
		sim:	1.000	0.366	0.172	0.041	0.010				Phe	(M - 85) <sup>+</sup>	sim:	1.000	0.289	0.108	0.020	0.003	0.000	0.000	0.000	0.000	0.000
Glx	(M - 85) <sup>+</sup>	exp:	1.000	0.339	0.165	0.038						(M - 159) <sup>+</sup>	exp:	1.000	0.208	0.057	0.008	0.003	0.002	0.005	0.000	0.003	0.000
		sim:	1.000	0.354	0.166	0.039						(f302) <sup>+</sup>	sim:	1.000	0.215	0.057	0.007	0.001	0.000	0.000	0.000	0.000	0.000
	(f302) <sup>+</sup>	exp:	1.000	0.271	0.106	0.031						(f302) <sup>+</sup>	exp:	1.000	0.263	0.104							
		sim:	1.000	0.280	0.110	0.020						(f302) <sup>+</sup>	sim:	1.000	0.268	0.104							
Ile	(M - 57) <sup>+</sup>	exp:	1.000	0.259	0.105							sc <sup>+</sup>	exp:	1.000	0.092	0.000	0.000	0.000	0.000	0.000	0.000	0.000	0.000
		sim:	1.000	0.268	0.104							(M - 57) <sup>+</sup>	sim:	1.000	0.079	0.003	0.000	0.000	0.000	0.000	0.000	0.000	0.000
	(M - 85) <sup>+</sup>	exp:	1.000	0.363	0.170	0.041	0.010	0.000			Pro	(M - 57) <sup>+</sup>	exp:	1.000	0.250	0.104	0.027	0.017	0.007				
		sim:	1.000	0.377	0.176	0.043	0.010	0.002			Pro	(M - 85) <sup>+</sup>	sim:	1.000	0.256	0.101	0.017	0.003	0.000				
Gly	(M - 85) <sup>+</sup>	exp:	1.000	0.351	0.166	0.046	0.015					(M - 85) <sup>+</sup>	exp:	1.000	0.245	0.096	0.015	0.003					
		sim:	1.000	0.366	0.170	0.041	0.010					(M - 159) <sup>+</sup>	sim:	1.000	0.159	0.045	0.005	0.011					
	(f302) <sup>+</sup>	exp:	1.000	0.284	0.105	0.020	0.004					(M - 57) <sup>+</sup>	exp:	1.000	0.170	0.048	0.005	0.000					
		sim:	1.000	0.292	0.113	0.021	0.004					(M - 57) <sup>+</sup>	sim:	1.000	0.350	0.164	0.044	0.000					
Leu	(M - 57) <sup>+</sup>	exp:	1.000	0.294	0.113							(M - 159) <sup>+</sup>	exp:	1.000	0.354	0.166	0.039						
		sim:	1.000	0.268	0.104							(f302) <sup>+</sup>	sim:	1.000	0.269	0.104							
	(M - 85) <sup>+</sup>	exp:	1.000	0.222	0.093							(f302) <sup>+</sup>	exp:	1.000	0.266	0.122							
		sim:	1.000	0.206	0.093							(M - 85) <sup>+</sup>	sim:	1.000	0.268	0.104							
Lys	(M - 85) <sup>+</sup>	exp:	1.000	0.272	0.124	0.028	0.008	0.004			Tyr	(M - 85) <sup>+</sup>	exp:	1.000	0.393	0.200	0.073	0.057	0.011	0.043	0.010	0.035	
		sim:	1.000	0.256	0.099	0.016	0.003	0.000			Tyr	(M - 159) <sup>+</sup>	sim:	1.000	0.410	0.185	0.048	0.011	0.002	0.000	0.000	0.000	
	(M - 159) <sup>+</sup>	exp:	1.000	0.176	0.052	0.004	0.001	0.000				(M - 159) <sup>+</sup>	exp:	1.000	0.339	0.165	0.071	0.000	0.053	0.006	0.058	0.040	
		sim:	1.000	0.182	0.050	0.005	0.000	0.000				(f302) <sup>+</sup>	sim:	1.000	0.336	0.124	0.026	0.005	0.001	0.000	0.000	0.000	
Val	(M - 85) <sup>+</sup>	exp:	1.000	0.269	0.104	0.018	0.005	0.001				(f302) <sup>+</sup>	exp:	1.000	0.272	0.106							
		sim:	1.000	0.256	0.099	0.016	0.003	0.000				(M - 57) <sup>+</sup>	sim:	1.000	0.268	0.104							
	(M - 159) <sup>+</sup>	exp:	1.000	0.182	0.058	0.009	0.002	0.066				(M - 57) <sup>+</sup>	exp:	1.000	0.248	0.094	0.019	0.003	0.005				
		sim:	1.000	0.182	0.050	0.005	0.000	0.000				(M - 85) <sup>+</sup>	sim:	1.000	0.256	0.101	0.017	0.003	0.000				
Val	(M - 57) <sup>+</sup>	exp:	1.000	0.402	0.189	0.054	0.035	0.009	0.036			(M - 85) <sup>+</sup>	exp:	1.000	0.264	0.099	0.018	0.000					
		sim:	1.000	0.381	0.173	0.042	0.010	0.002	0.000			(M - 85) <sup>+</sup>	sim:	1.000	0.245	0.096	0.015	0.003					
	(M - 159) <sup>+</sup>	exp:	1.000	0.327	0.135	0.046	0.034	0.009				(f302) <sup>+</sup>	exp:	1.000	0.263	0.104							
		sim:	1.000	0.295	0.110	0.020	0.003	0.000				(f302) <sup>+</sup>	sim:	1.000	0.268	0.104							

<sup>a</sup> Fractions of different mass isotopomers (mx) are normalized to the base fragment (m0), where x denotes the increased molecular weight in atom mass units.

or in short terminology

$$\text{MDV}_{aa,\text{total}} = \text{MMM}_{aa,\text{total}} \cdot \text{IDV}_{aa} \quad (5)$$

The number of independent constraints (NIC) on the isotopomer distribution of amino acid *aa* was identified by inspection of the resulting total  $\text{MMM}_{aa,\text{total}}$  and was equal to its rank:

$$\text{NIC}_{aa} = \text{rank}(\text{MMM}_{aa,\text{total}}) \quad (6)$$

The isotopomer constitution of two amino acids, serine and glycine, was resolved completely, and for alanine only two degrees of freedom remained. In total, 125 independent constraints on the 1508 isotopomers of the 16 considered amino acids were accessible by our analysis (Table 2).

### Discussion

Tracer experiments represent a powerful tool for the investigation of metabolic reaction networks (2, 8, 26, 27). For the analysis of such experiments, the isotopomer balancing framework (5–7) enables a comprehensive mathematical description of labeling pattern in complex metabolic systems. Hence, it constitutes a conceptual extension of tracer analysis and the call is now open for experimental methods—analytical techniques (28) and optimized mixtures of labeled tracer molecule (29)—that rapidly provide a maximum of information. Instead of using single, analytical equations for labeling data interpretation, these massive data sets require fitting procedures and statistical analysis (30). Although many publications report on the use of NMR data (3, 8, 9), an experimental GC–MS method was reported for the comprehensive use of mass isotopomer data was reported only very recently (10). This particular GC–MS method has a faster amino acid separation procedure but requires a higher experimental effort because three derivatization methods were used. For metabolic flux analysis, this method yields a total of 91 constraints on the amino acid isotopomer pool, compared to 125 constraints in our analysis. While the lower number of constraints may be compensated by a higher precision of the selected ion monitoring mode that was selected for MS detection, our simulations show sufficient accuracy of the electron impact ionization mode. Thus, we present a fast and reliable GC–MS procedure for metabolic flux analysis that generates many independent constraints in a single experiment.

Another aim of this study was to deliver a suitable interface for the use of mass isotopomer data within an isotopomer balancing framework. In this context, it is a prerequisite to account for the skewing effects of natural isotopes. This can be achieved by two approaches. The first makes use of experimental data and requires the construction of a series of enrichment calibration curves (31), which requires experimental efforts and suffers from the limited availability of increasingly labeled standards. The second is based on simulating the reported or estimated natural occurrence of elemental isotopes. Fernandez and co-workers (32) described the correction of di-TBDMS-derivatized pyruvate mass distributions by a computed correction matrix. However, no information on matrix construction was given. Wittmann and Heinzle (22) developed a method to correct simulated carbon skeleton mass distributions for the natural isotope abundances of the other contained elements. In addition to this correction, however, skewing effects of elements with more than two major isotopes (e.g., O and Si) cannot

**Table 2. Accessible Independent Constraints on the Isotopomer Distribution by Different  $^{13}\text{C}$  Amino Acid Analysis Methods**

amino acid	no. of isotopomers	constraints on isotopomer pool		
		MS <sup>a</sup>	COSY <sup>b</sup>	FE <sup>c</sup>
Ala	8	6	4	2
Arg	64		5	
Asx	16	10	6	2
Glx	32	12	8	3
Gly	4	4	1	2
His	64		7	
Ile	64	6	7	3
Leu	64	6	7	5
Lys	64	14	7	5
Met	32	10	3	
Phe	512	18	6	2
Pro	32	10	8	
Ser	8	8	4	2
Thr	16		6	3
Tyr	512	11	10	
Val	16	10	5	2

<sup>a</sup> Based on the accepted fragments in Table 1. <sup>b</sup> Correlation spectroscopy; data taken from ref 3. <sup>c</sup> Fractional enrichment; data taken from ref 8.

be treated independently. Here we developed a general, matrix-based method that allows automatic generation of mass mapping matrices. Moreover, in contrast to similar GC–MS methods (10, 22, 33), we calculate the mass isotopomer distributions from the isotopomer distributions in one step. This reduces computation and thus improves the performance of the computation-intensive iterative fitting procedure for metabolic flux analysis.

The good agreement between experimentally determined and simulated results (Table 1) proves the capability of the presented method to accurately describe experimental and literature data on natural isotope abundances. The influence of altered isotope abundances in the range observed in nature (25) are negligible, compared to the changes that arise from different flux conditions. Thus, the natural isotope abundance does not need to be adjusted/estimated for flux analysis, provided acceptable results are obtained with samples that are labeled at natural abundance.

Simulations with a simplified metabolic isotopomer model indicate that the proposed GC–MS procedure provides valuable information for metabolic flux analysis by isotopomer balancing. However, a definite answer on whether a particular flux can be quantified by a particular procedure can only be given for a defined network and a defined operating region after extended analysis (6, 30). General properties of an analytical procedure are, nevertheless, important to provide a rough impression on its potential and to compare it to other methods. In this context, the number of independent constraints on the isotopomer distribution is very important. In the case of NMR-detected  $^{13}\text{C}$  enrichments, an amino acid with  $n$   $^{13}\text{C}$  nuclei,  $m$  of them being measured, yields  $m$  constraints on its isotopomer pool, with  $m \leq n$ . The situation is more complex for COSY NMR analysis of amino acids, where proton-bound carbon atoms can either be centrally or peripherally located. Peripheral carbon atoms provide one linear constraint on the amino acid isotopomer pool, because two isotopomeric patterns are observable. Two to three constraints can be deduced for centrally located carbon atoms, depending on whether different scalar coupling constants exist (3). Of all three analyses, only GC–MS analysis is theoretically capable to resolve all amino acid isotopomers. As illustrated in Table 2, the GC–MS methodology presented here yields more inde-

pendent constraints than either of the two NMR methods and even resolves the complete isotopomer composition of two amino acids, serine and glycine. The complete isotopomer constitution of additional amino acids may be accessible by GC-MS if additional derivatization methods with alternative cracking patterns are used (10, 34).

### Acknowledgment

This work was supported by a scholarship from the Boehringer Ingelheim Fonds to M.D.

### References and Notes

- (1) Bailey, J. E. Toward a science of metabolic engineering. *Science* **1991**, *252*, 1668–1675.
- (2) Szyperski, T.  $^{13}\text{C}$  NMR, MS and metabolic flux balancing in biotechnology research. *Q. Rev. Biophys.* **1998**, *31*, 41–106.
- (3) Szyperski, T. Biosynthetically directed fractional  $^{13}\text{C}$ -labeling of proteinogenic amino acids. An efficient analytical tool to investigate intermediary metabolism. *Eur. J. Biochem.* **1995**, *232*, 433–448.
- (4) Sauer, U.; Lasko, D. R.; Fiaux, J.; Hochuli, M.; Glaser, R.; Szyperski, T.; Wüthrich, K.; Bailey, J. E. Metabolic flux ratio analysis of genetic and environmental modulations of *Escherichia coli* central carbon metabolism. *J. Bacteriol.* **1999**, *181*, 6679–6688.
- (5) Zupke, C.; Stephanopoulos, G. Modeling of isotope distributions and intracellular fluxes in metabolic networks using atom mapping matrices. *Biotechnol. Prog.* **1994**, *10*, 489–498.
- (6) Wiechert, W.; de Graaf, A. A. Bidirectional reaction steps in metabolic networks: I. Modeling and simulation of carbon isotope labeling experiments. *Biotechnol. Bioeng.* **1997**, *55*, 101–117.
- (7) Schmidt, K.; Carlsen, M.; Nielsen, J.; Villadsen, J. Modeling isotopomer distributions in biochemical networks using isotopomer mapping matrices. *Biotechnol. Bioeng.* **1997**, *55*, 831–840.
- (8) Marx, A.; de Graaf, A. A.; Wiechert, W.; Eggeling, L.; Sahm, H. Determination of the fluxes in the central metabolism of *Corynebacterium glutamicum* by nuclear magnetic resonance spectroscopy combined with metabolite balancing. *Biotechnol. Bioeng.* **1996**, *49*, 111–129.
- (9) Schmidt, K.; Norregaard, L. C.; Pedersen, B.; Meissner, A.; Duus, J. O.; Nielsen, J. O.; Villadsen, J. Quantification of intracellular metabolic fluxes from fractional enrichment and  $^{13}\text{C}$ - $^{13}\text{C}$  coupling constraints on the isotopomer distribution in labeled biomass components. *Met. Eng.* **1999**, *1*, 166–179.
- (10) Christensen, B.; Nielsen, J. Isotopomer analysis using GC-MS. *Met. Eng.* **1999**, *1*, 282–290.
- (11) Poole, C. F.; Sye, W.-F.; Singhawangcha, S.; Hsu, F.; Zlatkis, A.; Arfwidsson, A.; Vessman, J. New electron-capturing pentafluorophenyldialkylchlorosilanes as versatile derivatizing reagents for gas chromatography. *J. Chromatogr.* **1980**, *199*, 123–142.
- (12) Evershed, R. P. Advances in silylation. In *Handbook of Derivatives for Chromatography*; Blau, K., Halket, J. M. Eds.; John Wiley & Sons: New York, 1993; pp 51–108.
- (13) Kellner, R.; Meyer, H. E.; Lottspeich, F. Amino acid analysis. In *Microcharacterization of Proteins*; Kellner, R., Lottspeich, F., Meyer, H. E., Eds.; Wiley-VCH: Weinheim, 1999; pp 119–140.
- (14) Bentley, R.; Saha, N. C.; Sweeley, C. C. Separation of protium and deuterium forms of carbohydrates by gas chromatography. *Anal. Chem.* **1965**, *37*, 1118–1122.
- (15) Goromaru, T.; Maeda, H. Isotopic fractionation of isopropylantipyrine and its deuterated analogues by capillary gas chromatography. *Biol. Pharm. Bull.* **1994**, *17*, 1635–1639.
- (16) Das Neves, H. J. C.; Vasconcelos, A. M. P. Capillary gas chromatography of amino acids, including asparagine and glutamine: sensitive gas chromatographic-mass spectrometric and selected ion monitoring gas chromatographic-mass spectrometric detection of the *N,O(S)*-tert.-butyldimethylsilyl derivatives. *J. Chromatogr.* **1987**, *392*, 249–258.
- (17) Hellerstein, M. K.; Neese, R. A. Mass isotopomer distribution analysis at eight years: theoretical, analytic, and experimental considerations. *Am. J. Physiol.* **1999**, *276*, E1146–1170.
- (18) Mook, W. G.; Grootes, P. M. The measuring procedure and corrections for the high-precision mass-spectrometric analysis of isotopic abundance ratios, especially referring to carbon, oxygen and nitrogen. *Int. J. Mass Spectrom. Ion Phys.* **1973**, *12*, 273–298.
- (19) Bergner, E. A.; Lee, W.-N. P. Testing gas chromatographic/mass spectrometric systems for linearity of response. *J. Mass Spectrom.* **1995**, *30*, 778–780.
- (20) Fagerquist, C. K.; Neese, R. A.; Hellerstein, M. K. Molecular ion fragmentation and its effects on mass isotopomer abundances of fatty acid methyl esters ionized by electron impact. *J. Am. Soc. Mass Spectrom.* **1999**, *10*, 430–439.
- (21) Wiechert, W.; Möllney, M.; Isermann, N.; Wurzel, M.; de Graaf, A. A. Bidirectional reaction steps in metabolic networks: III. Explicit solution and analysis of isotopomer labeling systems. *Biotechnol. Bioeng.* **1999**, *66*, 69–85.
- (22) Wittmann, C.; Heinzle, E. Mass spectrometry for metabolic flux analysis. *Biotechnol. Bioeng.* **1999**, *62*, 739–750.
- (23) Wood, T. *The Pentose Phosphate Pathway*; Academic Press: Orlando, 1985.
- (24) Sauer, U.; Hatzimanikatis, V.; Hohmann, H. P.; Manneberg, M.; van Loon, A. P.; Bailey, J. E. Physiology and metabolic fluxes of wild-type and riboflavin-producing *Bacillus subtilis*. *Appl. Environ. Microbiol.* **1996**, *62*, 3687–96.
- (25) Deines, P. The isotopic composition of reduced organic carbon. In *Handbook of Environmental Isotope Geochemistry. The Terrestrial Environment*; Fritz, P., Fontes, J. C., Eds.; Elsevier: Amsterdam, 1980; Vol. 1, Chapter 9.
- (26) Sauer, U.; Hatzimanikatis, V.; Bailey, J. E.; Hochuli, M.; Szyperski, T.; Wüthrich, K. Metabolic fluxes in riboflavin-producing *Bacillus subtilis*. *Nat. Biotechnol.* **1997**, *15*, 448–452.
- (27) Christensen, B.; Nielsen, J. Metabolic network analysis. A powerful tool in metabolic engineering. *Adv. Biochem. Eng. Biotechnol.* **2000**, *66*, 209–31.
- (28) Sauer, U.; Szyperski, T.; Bailey, J. E. Future trends in complex microbial reaction studies. In *NMR in Microbiology: Theory and Applications*; Horizon Scientific Press: Wymondham, 2000; pp 483–494.
- (29) Möllney, M.; Wiechert, W.; Kownatzki, D.; de Graaf, A. A. Bidirectional reaction steps in metabolic networks: IV. Optimal design of isotopomer labeling experiments. *Biotechnol. Bioeng.* **1999**, *66*, 86–103.
- (30) Wiechert, W.; Siefke, C.; de Graaf, A.; Marx, A. Bidirectional reaction steps in metabolic networks: II. Flux estimation and statistical analysis. *Biotechnol. Bioeng.* **1997**, *55*, 118–135.
- (31) Peroni, O.; Large, V.; Beylot, M. Measuring gluconeogenesis with [ $2\text{-}^{13}\text{C}$ ]glycerol and mass isotopomer distribution analysis of glucose. *Am. J. Physiol.* **1995**, *269*, 516–523.
- (32) Fernandez, C. F.; Des Rosiers, C.; Previs, S. F.; David, F.; Brunengraber, H. Correction of  $^{13}\text{C}$  mass isotopomer distributions for natural stable isotope abundance. *J. Mass Spectrom.* **1996**, *31*, 255–262.
- (33) Chinkes, D. L.; Aarsland, A.; Rosenblatt, J.; Wolfe, R. R. Comparison of mass isotopomer dilution methods used to compute VLDL production in vivo. *Am. J. Physiol.* **1996**, *271*, E373–383.
- (34) Husek, P. Amino acid derivatization and analysis in five minutes. *FEBS Lett.* **1991**, *280*, 354–356.

Accepted for publication May 24, 2000.

BP000058H